High-fidelity sensitivity analysis of modal properties of mistuned bladed disks regarding material anisotropy

Article (Accepted Version)

Proceedings of ASME Turbo Expo 2018: Turbomachinery Technical Conference and Exposition
GT2018
June 11-15, 2018, Oslo, Norway

GT2018-76572

HIGH-FIDELITY SENSITIVITY ANALYSIS OF MODAL PROPERTIES OF MISTUNED BLADED DISKS REGARDING MATERIAL ANISOTROPY

Adam Koscso

School of Engineering and Informatics
University of Sussex
Brighton, United Kingdom, BN1 9QT
Email: adam.koscso@sussex.ac.uk

Guido Dhondt

MTU Aero Engines AG
Dachauer Strasse 665
80995 Munich, Germany
Email: guido.dhondt@mtu.de

E.P. Petrov

School of Engineering and Informatics
University of Sussex
Brighton, United Kingdom, BN1 9QT
Email: y.petrov@sussex.ac.uk

ABSTRACT

A new method has been developed for sensitivity calculations of modal characteristics of bladed disks made of anisotropic materials. The method allows the determination of the sensitivity of the natural frequencies and mode shapes of mistuned bladed disks with respect to anisotropy angles that define the crystal orientation of the monocrystalline blades using full-scale finite element models. An enhanced method is proposed to provide high accuracy for the sensitivity analysis of mode shapes. An approach has also been developed for transforming the modal sensitivities to coordinate systems used in industry for description of the blade anisotropy orientations.

The capabilities of the developed methods are demonstrated on examples of a single blade and a mistuned realistic bladed disk finite element models. The modal sensitivity of mistuned bladed disks to anisotropic material orientation is thoroughly studied.

INTRODUCTION

In the turbine stages of jet engines and gas turbines single crystal and directionally solidified materials have been applied in order to withstand the high pressure, extreme temperature regimes and large centrifugal forces. By a carefully controlled casting process, it can be achieved that the single crystal materials only consist of one type of columnar grain. This leads to the disappearance of the grain boundaries between the crystals and to all crystals facing in the same direction. Because of this, the single crystal materials have anisotropic elastic constants, however, the face-centered cubic structure of the nickel based superalloys introduces additional symmetry. The application of the single crystal and directionally solidified materials provides superior creep resistance and fatigue life extension mainly due to the disappearance of the grain boundaries. The analysis of this feature has been studied extensively in the literature (see Refs. [1] and [2]).

The main growing direction of the single crystals is carefully controlled during the casting process, however, the secondary crystal orientations are not. Therefore, the angles describing the orientations can take random values within certain limits and in most cases statistical distributions can also be derived. The publications on this topic have been investigating the static and dynamic response of single blades and bladed disks with different anisotropy orientations.

The static behavior of a tuned bladed disk has been investigated in Ref. [3], with special emphasis on the stress state on the contact interfaces between the single crystal blade and isotropic disk. The simulations in that paper have been carried out with 81 different crystal orientations, and showed a deviation of +9.7% and -19% in normalized maximum principle stress compared with the orientation when the material coordinate system coincides with the blade coordinate system.

The influence of the crystal orientation on the natural frequencies of the turbine buckets has been analyzed in Ref. [4] by experimental and computational means. By using the surface response method a natural frequency variation of less than 4% has

been concluded for the first ten free-free modes.

Kaneko, [5] working with simple plate models, showed the effect of angle deviation on the natural frequencies for the first ten modes in the case of single crystal and directionally solidified materials.

In the more recent publication of Kaneko [6], the variation of the resonant and random response due to changes of anisotropy orientation and material constants, in case of a realistic mistuned bladed disk model with directionally solidified blades was analyzed. The simulations utilized sensitivities and the Monte Carlo method for calculating the forced response with the help of a fundamental mistuning model (see Ref. [7]).

A comprehensive review of the methodology for calculating the derivative of the eigenvalues and eigenvectors has been published by Adelman and Haftka in Ref. [8].

In the current work a semi-analytical method is proposed for the sensitivity analysis of the natural frequencies and mode shapes of a bladed disk with respect to the anisotropy angles describing the crystal orientations. An enhanced method is proposed for the calculation of the sensitivity of mode shapes in order to achieve fast convergence and highly accurate results.

The sensitivities calculated with respect to the rotation vector components defined in the global coordinate system must be transformed with respect to the manufacturers anisotropy angles defined in the local coordinate system of the blade. For this, an analytically derived facility is proposed.

The variation of the natural frequencies and mode shapes due to different realistic crystal orientations have been calculated for single blade and mistuned bladed disks. The sensitivity method has been validated using single blade and full model of bladed disk.

The effect of the anisotropy orientation on a realistic bladed disk is presented with a thorough study of the sensitivity of modal characteristics.

MODELING AND METHOD

Linear Elastic Stress and Strain of Single Crystal Materials

The single crystal materials used in modern blades have directionally dependent elastic constants. The crystals of modern nickel-base superalloys are organized in a face centered cubic crystal structure, which introduces additional symmetry in the material, therefore there are only three independent elasticity constants. The cubic materials are a subset of orthotropic materials because the shear modulus G_0 is independent of Young's modulus E_0 and Poisson's ratio ν_0.

The compliance matrix in the stress-strain relation $\boldsymbol{\varepsilon} = \boldsymbol{S}\boldsymbol{\sigma}$, using the Voigt notation, for a nickel base superalloy is defined as Eq. (1). Where the constants are: $S_{33} = 1/E_0$, $S_{13} = -\nu_0/E_0$ and $S_{44} = 1/G_0$.

$$\boldsymbol{S} = \begin{bmatrix} S_{33} & S_{13} & S_{13} & 0 & 0 & 0 \\ S_{13} & S_{33} & S_{13} & 0 & 0 & 0 \\ S_{13} & S_{13} & S_{33} & 0 & 0 & 0 \\ 0 & 0 & 0 & S_{44} & 0 & 0 \\ 0 & 0 & 0 & 0 & S_{44} & 0 \\ 0 & 0 & 0 & 0 & 0 & S_{44} \end{bmatrix} \tag{1}$$

The compliance matrix has the form shown in Eq. (1) only if the material and the blade coordinate systems (CS) are coinciding however, the blade and material coordinate systems usually differ. After the blades are manufactured, the crystal orientation of each blade is usually measured by the Laue method [9] and the anisotropy angles describing the crystal orientation of each blade of the mistuned bladed disk are provided in the local CS of the blades.

In Fig. 1 the material coordinate system axes are denoted as [100], [010] and [001], the blade CS axes as x', y' and z', and the global CS axes as X, Y and Z. The imperfect crystal growth during the manufacturing process leads to the deviation of the material CS with respect to the blade CS and causes anisotropy mistuning in a bladed disk. In this case, the compliance matrix described in the blade CS can be calculated with the multiplication of the initial compliance matrix with the stress transformation matrix $\boldsymbol{Q}$ from the right and with its transpose $\boldsymbol{Q}^T$ from the left as shown in Eq. (2).

$$\boldsymbol{S}^*(\boldsymbol{R}_M) = \boldsymbol{Q}^T(\boldsymbol{R}_M)\,\boldsymbol{S}\,\boldsymbol{Q}(\boldsymbol{R}_M) \tag{2}$$

The definition of the stress transformation matrix $\boldsymbol{Q}$ is based on the rotation matrix $\boldsymbol{R}_M$ that describes the transformation from the material CS to the blade CS. The rotation of the coordinate system from the initial single-crystal material CS to the CS of the blade is carried out with rotation matrices. Because this rotation is executed in 3D space, it can be described with three independent variables.

Anisotropy Description in Global Coordinate System

For the calculations of the modal properties and their sensitivities the finite element matrices are obtained in the global CS.

The material CS describing the crystal orientation of each blade in the global CS is defined by the rotation vector:

$$\boldsymbol{v} = \begin{bmatrix} v_x \\ v_y \\ v_z \end{bmatrix} \tag{3}$$

The rotation matrix can be then expressed as:

$$\boldsymbol{R}(\boldsymbol{v}) = \boldsymbol{I} + \frac{\sin(\|\boldsymbol{v}\|)}{\|\boldsymbol{v}\|}\widetilde{\boldsymbol{\omega}}_{\boldsymbol{v}} + \frac{1-\cos(\|\boldsymbol{v}\|)}{\|\boldsymbol{v}\|^2}\widetilde{\boldsymbol{\omega}}_{\boldsymbol{v}}\widetilde{\boldsymbol{\omega}}_{\boldsymbol{v}} \tag{4}$$

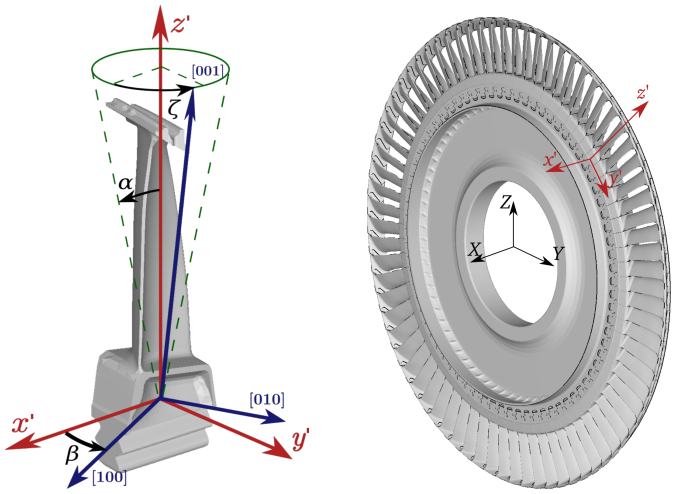

(a) Definition of the material and blade CS

(b) Blade CS in the global CS

FIGURE 1: Definition of the material and blade coordinate system

Where, $\widetilde{\boldsymbol{\omega}}_{\boldsymbol{v}}$ is the skew-symmetric matrix defined in the global coordinate system by the rotation vector components as:

$$\widetilde{\boldsymbol{\omega}}_{\boldsymbol{v}} = \begin{bmatrix} 0 & -v_z & v_y \\ v_z & 0 & -v_x \\ -v_y & v_x & 0 \end{bmatrix} \tag{5}$$

and $\boldsymbol{I}$ is the identity matrix.

Manufacturer Anisotropy Angles Description

The anisotropy angles defined in the CS of each blade,

$$\boldsymbol{\Gamma} = \{\alpha, \beta, \zeta\} \tag{6}$$

are shown in Fig. 1a. The primary angle, the deviation of [001] axis with respect to is z' axis, is represented by α. The secondary angle β is defined as the smaller angle between x' axis and [100] or x' axis and [010]. The third angle ζ defines the position of the [001] axis on a circle defined parallel to the $x'-y'$ plane. The angle ζ can take any value between $-180°$ and $180°$, however if $\alpha = 0$, the value of the circular angle is undefined.

In the current practice, this description is provided by the blade manufacturer and it is based on the Euler rotations, therefore all angles are defined as a rotation about coordinate axes in a certain order. First, the secondary rotation with the angle $\beta^* = \beta - \zeta$ about the axis z' is performed. Second, the primary rotation about y' axis is executed with the value of α. Third, the rotation with angle ζ about axis z' is realized. By carrying out the three rotations with angles α, β and ζ the transformation between the material CS and blade CS is defined:

$$\boldsymbol{R}_M(\boldsymbol{\Gamma}) = \boldsymbol{R}_\zeta \boldsymbol{R}_\alpha \boldsymbol{R}_{\beta^*} \tag{7}$$

The rotation matrix $\boldsymbol{R}_G(\boldsymbol{\Gamma})$, describing the blade material orientation in the global CS depends on the location of the blade in the bladed disk assembly (see Fig. 1b), which is characterized by the blade orientation rotation matrix $\boldsymbol{R}_B$ describing blade stacking position, and a rotation matrix describing material orientation with respect to blade stacking position, $\boldsymbol{R}_M(\boldsymbol{\Gamma})$. Therefore, $\boldsymbol{R}_G(\boldsymbol{\Gamma})$ takes the form:

$$\boldsymbol{R}_G(\boldsymbol{\Gamma}) = \boldsymbol{R}_B \boldsymbol{R}_M(\boldsymbol{\Gamma}) \tag{8}$$

Sensitivity of Eigenvalues of Multi-Degree-of-Freedom Dynamic Systems

In order to calculate the sensitivities with respect to the crystal orientation variation, the derivatives of the modal characteristics have to be calculated with respect to the variables describing the coordinate system rotation.

The eigenvalue problem of the multi-degree-of-freedom (MDOF) dynamic system can be written as:

$$\boldsymbol{K}\boldsymbol{\phi}_j = \lambda_j \boldsymbol{M}\boldsymbol{\phi}_j \tag{9}$$

Where, the stiffness matrix $\boldsymbol{K}$, the eigenvalues λ_j and the mode shapes, $\boldsymbol{\phi}_j$, are dependent on the anisotropy angles, but the mass matrix $\boldsymbol{M}$ is not, and the subscript j is the mode number. The geometric stiffening effects of the centrifugal forces of a rotating bladed disk assembly can be considered in the stiffness matrix $\boldsymbol{K}$.

In order to calculate the sensitivities of the eigenvalues, differentiating the governing equation Eq. (9) is necessary. For this derivation, the parameter γ is introduced as a general parameter that can be any parameter describing the orientation of the single crystal material. Assuming mass-normalized eigenvectors, $\boldsymbol{\phi}_j$, the equation describing the sensitivity of the eigenvalues for a MDOF dynamic system takes the form [8] :

$$\frac{\partial \lambda_j}{\partial \gamma} = \boldsymbol{\phi}_j^T \left(\frac{\partial \boldsymbol{K}}{\partial \gamma} - \lambda_j \frac{\partial \boldsymbol{M}}{\partial \gamma} \right) \boldsymbol{\phi}_j \tag{10}$$

Since the mass matrix is not dependent on γ, this expression becomes:

$$\frac{\partial \lambda_j}{\partial \gamma} = \boldsymbol{\phi}_j^T \frac{\partial \boldsymbol{K}}{\partial \gamma} \boldsymbol{\phi}_j \tag{11}$$

The sensitivities of the natural frequency f_j in Hz can be expressed as:

$$\frac{\partial f_j}{\partial \gamma} = \frac{\partial \lambda_j}{\partial \gamma} \cdot \frac{1}{4 \cdot \pi \cdot \sqrt{\lambda_j}} \tag{12}$$

The derivative of the stiffness matrix in Eq. (11), with respect to the anisotropy angle for linear calculations can be calculated using an analytical method. The sensitivity of the stiffness matrix

on the element level can be expressed with the modified equation of the element stiffness formulation of a three dimensional isoparametric finite element as:

$$\frac{\partial \boldsymbol{k}^e}{\partial \gamma} = \int_{V^e} \boldsymbol{B}^T \frac{\partial \boldsymbol{C}^*}{\partial \gamma} \boldsymbol{B} dV \tag{13}$$

Where $\boldsymbol{k}^e$ is the finite element stiffness matrix, $\boldsymbol{C}^*$ is the elasticity matrix defined in the global coordinate system, $\boldsymbol{B}$ is the strain-displacement matrix and V^e is the volume of the element. In order to carry out the calculation described in Eq.(13) the derivative of the elasticity matrix is calculated.

The transformation of the elasticity matrix from the single crystal coordinate system to the global coordinate system can be described as Eq. (14), where $\boldsymbol{Q}$ is the stress transformation matrix, dependent on $(\boldsymbol{R}_G)$, and $\boldsymbol{C}$ is the inverse of the compliance matrix $\boldsymbol{S}$ defined in Eq. (1).

$$\boldsymbol{C}^* = \boldsymbol{Q}\boldsymbol{C}\boldsymbol{Q}^T \tag{14}$$

Taking the derivative of the elasticity matrix in the global CS results in:

$$\frac{\partial \boldsymbol{C}^*}{\partial \gamma} = \frac{\partial \boldsymbol{Q}}{\partial \gamma}\boldsymbol{C}\boldsymbol{Q}^T + \boldsymbol{Q}\boldsymbol{C}\frac{\partial \boldsymbol{Q}^T}{\partial \gamma}. \tag{15}$$

In the open-source finite element package of CalculiX [10], a forward-difference formula is implemented for this purpose. The application of this formula requires two evaluations of the stiffness matrix. One with the unperturbed anisotropy parameters and one when one of the parameters is increased with a sufficiently small $\Delta\gamma$ finite difference step.

$$\frac{\partial \boldsymbol{k}^e(\gamma)}{\partial \gamma} \approx \frac{\boldsymbol{k}^e(\gamma+\Delta\gamma) - \boldsymbol{k}^e(\gamma)}{\Delta\gamma} \tag{16}$$

For efficiency, the right hand side term in Eq. (11) is calculated on the element level, leading to:

$$\boldsymbol{\phi}_j^T \frac{\partial \boldsymbol{K}}{\partial \gamma}\boldsymbol{\phi}_j = \boldsymbol{\phi}_j^T \left(\bigcup_e \frac{\partial \boldsymbol{k}^e}{\partial \gamma}\boldsymbol{\phi}_j{}^e \right). \tag{17}$$

The governing equation of the mechanical problem has been derived analytically until Eq. (11). The sensitivity of the stiffness matrix, however, is calculated by numerical means. Therefore, the method is semi-analytic.

Enhanced Method for the Sensitivity of Mode Shape Calculation

In order to express the sensitivity of mode shapes, a series expansion formulation is traditionally used e.g. see Ref. [8]

$$\frac{\partial \boldsymbol{\phi}_j}{\partial \gamma} = \sum_{k=1}^{m} c_{jk}\boldsymbol{\phi}_k = \boldsymbol{\Phi}\boldsymbol{c}_j \tag{18}$$

The formulation in Eq. (18) considers only a subset of mode shapes m in the expansion of the derivative of the mode shapes. In order to increase the precision and the speed of convergence an enhanced method is proposed. This approach accounts for the mode shapes that are not included in the expansion, in the form of a residual vector $\boldsymbol{r}_j$.

$$\frac{\partial \boldsymbol{\phi}_j}{\partial \gamma} = \boldsymbol{\Phi}\boldsymbol{c}_j + \boldsymbol{r}_j \tag{19}$$

The coefficients of the first term on the right hand side of Eq. (19), $\boldsymbol{c}_j$, can be derived by first substituting Eq. (18) into the total derivative of Eq. (9) with respect to the general anisotropy parameter γ:

$$(\boldsymbol{K} - \lambda_j \boldsymbol{M})\boldsymbol{\Phi}\boldsymbol{c}_j = \boldsymbol{f}_j \tag{20}$$

where the right hand side for a general case is:

$$\boldsymbol{f}_j = -\left(\frac{\partial \boldsymbol{K}}{\partial \gamma} - \lambda_j \frac{\partial \boldsymbol{M}}{\partial \gamma} - \frac{\partial \lambda_j}{\partial \gamma}\boldsymbol{M} \right)\boldsymbol{\phi}_j \tag{21}$$

Then the components c_{jk} of the vector of the sensitivity expansion coefficients for j-th mode shape $\boldsymbol{c}_j$ are obtained for $k \neq j$ by multiplying Eq. (20) with the k^{th} mass-normalized mode shape $\boldsymbol{\phi}_k^T$ from the left. The coefficient c_{jj} is calculated by differentiating the normalization condition: $\boldsymbol{\phi}_j^T \boldsymbol{M}\boldsymbol{\phi}_j = 1$, which for a general case gives:

$$c_{jj} = -0.5\boldsymbol{\phi}_j^T \frac{\partial \boldsymbol{M}}{\partial \gamma}\boldsymbol{\phi}_j \tag{22}$$

For the sensitivity analysis to material anisotropy orientation, considered in this paper, the dependence of the mass matrix on the anisotropy orientation can be neglected. Therefore, Eq. (21) takes the following form:

$$\boldsymbol{f}_j = -\left(\frac{\partial \boldsymbol{K}}{\partial \gamma} - \frac{\partial \lambda_j}{\partial \gamma}\boldsymbol{M} \right)\boldsymbol{\phi}_j \tag{23}$$

The coefficients of the mode shape sensitivity expansion, considering that the mass matrix is not dependent on γ, result in:

$$c_{jk} = \begin{cases} \frac{\boldsymbol{\phi}_k^T \boldsymbol{f}_j}{\lambda_k - \lambda_j} & \text{if } k \neq j \\ 0 & \text{if } k = j \end{cases} \tag{24}$$

The residual vector in Eq. (19) should take into account the contribution of the modes which are truncated in Eq. (18)

$$\boldsymbol{r}_j = \sum_{k=m+1}^{N} \frac{\boldsymbol{\phi}_k^T \boldsymbol{f}_j}{\lambda_k - \lambda_j}\boldsymbol{\phi}_k \tag{25}$$

where N is the total number of modes in a considered structure (which is equal to the total number of DOFs in the finite element

model). In order to be able to calculate the residual vector, here some value λ_0 is substituted instead of λ_j. This value is chosen to be very close, but different from λ_j. Then the expression $\boldsymbol{r}_j$ can be divided into two terms as:

$$\boldsymbol{r}_j \approx \sum_{k=1}^{N} \frac{\boldsymbol{\phi}_k^T \boldsymbol{f}_j}{\lambda_k - \lambda_0} \boldsymbol{\phi}_k - \sum_{k=1}^{m} \frac{\boldsymbol{\phi}_k^T \boldsymbol{f}_j}{\lambda_k - \lambda_0} \boldsymbol{\phi}_k = \boldsymbol{r}_j^0 - \sum_{k=1}^{m} c_{jk}^r \boldsymbol{\phi}_k \quad (26)$$

The former term can be reformulated as a system of linear equations and therefore solved with a linear equation solver.

$$(\boldsymbol{K} - \lambda_0 \boldsymbol{M})\, \boldsymbol{r}_j^0 = \boldsymbol{f}_j \quad (27)$$

Substitution of Eq.(26) in Eq.(19) gives us the enhanced expression for the mode shape sensitivities:

$$\frac{\partial \boldsymbol{\phi}_j}{\partial \gamma} = \boldsymbol{\Phi} \boldsymbol{c}_j + \boldsymbol{r}_j^0 - \boldsymbol{\Phi} \boldsymbol{c}_j^r = \boldsymbol{\Phi} \boldsymbol{c}_j^* + \boldsymbol{r}_j^0 \quad (28)$$

The coefficients of the sensitivity of mode shapes using enhanced formulation in Eq. (28) can be calculated as:

$$c_{jk}^* = \begin{cases} \frac{\lambda_j - \lambda_0}{(\lambda_k - \lambda_j)(\lambda_k - \lambda_0)} \boldsymbol{\phi}_k^T \boldsymbol{f}_j & \text{if } k \neq j \\ -\frac{\boldsymbol{\phi}_k^T \boldsymbol{f}_j}{\lambda_k - \lambda_0} & \text{if } k = j \end{cases} \quad (29)$$

The value of λ_0 is selected sufficiently close to λ_j in order to allow accurate calculation, but far enough from λ_j to avoid singularities when solving the linear system of equations in Eq. (27). λ_0 can be chosen individually for each of the mode shapes of interest. For the case of calculation of sensitivities for a large number of mode shapes, in order to reduce the computational expense, λ_0 can be chosen the same for all mode shapes, which allows the calculation of sensitivities for all mode shapes with only one factorization of the matrix $(\boldsymbol{K} - \lambda_0 \boldsymbol{M})$ in Eq. (27). In this work, a different λ_0 reference frequency value is selected for each mode:

$$\lambda_0 = \frac{\lambda_j + \lambda_{j-1}}{2} \quad (30)$$

Calculation of the Sensitivities in Blade Coordinate System

The sensitivities of the finite element calculations are obtained with respect to the rotation vector components, defined in the global CS, but for assessment of the anisotropy effect the sensitivity with respect to measured experimental angles are needed. In order to calculate the sensitivities with respect to the anisotropy angles, the sensitivities to the rotation vectors have to be transformed into the blade coordinate system. The transformation can be carried out using the chain rule:

$$\frac{\partial a}{\partial \boldsymbol{\Gamma}} = \begin{bmatrix} \partial v_x/\partial\alpha & \partial v_y/\partial\alpha & \partial v_z/\partial\alpha \\ \partial v_x/\partial\beta & \partial v_y/\partial\beta & \partial v_z/\partial\beta \\ \partial v_x/\partial\zeta & \partial v_y/\partial\zeta & \partial v_z/\partial\zeta \end{bmatrix} \frac{\partial a}{\partial \boldsymbol{v}} = \frac{\partial \boldsymbol{v}}{\partial \boldsymbol{\Gamma}} \cdot \frac{\partial a}{\partial \boldsymbol{v}} \quad (31)$$

where a is any parameter of interest, and in this case this is natural frequency or modal displacement. The derivation of the Jacobian matrix, $\boldsymbol{J} = \partial \boldsymbol{v}/\partial \boldsymbol{\Gamma}$, was not available in the literature and is derived here by the authors in analytical form.

Calculation of the Transformation Matrix The expression derived for the Jacobian in Eq. (31) is based on the fact that the infinitesimal rotations expressed through rotation matrices of both coordinate systems: global CS and blade CS, should be identical. The infinitesimal rotation $\delta\boldsymbol{\omega} = \{\delta\omega_x, \delta\omega_y, \delta\omega_z\}$ can be expressed through the rotation matrix in the form (Ref. [11]):

$$\delta\widetilde{\boldsymbol{\omega}} = \delta\boldsymbol{R}\boldsymbol{R}^T \quad (32)$$

Substituting Eq. (8) in Eq. (32) the expression for infinitesimal rotations is obtained in through manufacturer material anisotropy angles in the form:

$$\begin{aligned} \delta\widetilde{\boldsymbol{\omega}} = \delta\boldsymbol{R}_G\boldsymbol{R}_G^T = \left(\boldsymbol{R}_B \frac{\partial \boldsymbol{R}_M}{\partial\alpha} \boldsymbol{R}_M^T \boldsymbol{R}_B^T\right) d\alpha + \\ \left(\boldsymbol{R}_B \frac{\partial \boldsymbol{R}_M}{\partial\beta} \boldsymbol{R}_M^T \boldsymbol{R}_B^T\right) d\beta + \left(\boldsymbol{R}_B \frac{\partial \boldsymbol{R}_M}{\partial\zeta} \boldsymbol{R}_M^T \boldsymbol{R}_B^T\right) d\zeta \end{aligned} \quad (33)$$

Taking into account that the matrix $\delta\widetilde{\boldsymbol{\omega}}$ obtained from Eq. (33) is a spin matrix (see Eq. (5)) and that each summand in Eq. (33) is a spin matrix, this equation can be rewritten in a vector form:

$$\delta\boldsymbol{\omega} = \boldsymbol{\omega}_\alpha \delta\alpha + \boldsymbol{\omega}_\beta \delta\beta + \boldsymbol{\omega}_\zeta \delta\zeta \quad (34)$$

On another side, the vector of infinitesimal rotations can be expressed through the rotation vector, $\boldsymbol{v}$, describing the material anisotropy in global CS. Using an available expression (see Refs. [11] and [12]), we have:

$$\delta\boldsymbol{\omega} = \boldsymbol{T}^T \delta\boldsymbol{v} \quad (35)$$

where the tangent operator matrix, $\boldsymbol{T}$, is expressed as:

$$\boldsymbol{T}(\boldsymbol{r}) = \boldsymbol{I} + \frac{\cos(\|\boldsymbol{v}\|) - 1}{\|\boldsymbol{v}\|^2} \widetilde{\boldsymbol{\omega}}_{\boldsymbol{v}} + \frac{\|\boldsymbol{v}\| - \sin(\|\boldsymbol{v}\|)}{\|\boldsymbol{v}\|^3} \widetilde{\boldsymbol{\omega}}_{\boldsymbol{v}} \widetilde{\boldsymbol{\omega}}_{\boldsymbol{v}} \quad (36)$$

Equalizing the terms upon independent variations of the rotation matrix parameters in Eqs. (34) and (35), we obtain the equations for the determination of the rows of the Jacobian matrix, $\boldsymbol{J}$, used for the transformation between the two coordinate systems: the global CS and blade CS:

$$\boldsymbol{T}^T \frac{\partial \boldsymbol{v}}{\partial\alpha} = \boldsymbol{\omega}_\alpha \;\;,\;\; \boldsymbol{T}^T \frac{\partial \boldsymbol{v}}{\partial\beta} = \boldsymbol{\omega}_\beta \;\;,\;\; \boldsymbol{T}^T \frac{\partial \boldsymbol{v}}{\partial\zeta} = \boldsymbol{\omega}_\zeta \quad (37)$$

NUMERICAL RESULTS

The new capabilities of the sensitivity of the modal characteristics with respect to the anisotropy orientation were applied to the analyses of a single blade and a full model of a realistic mistuned bladed disk shown in Fig. 2.

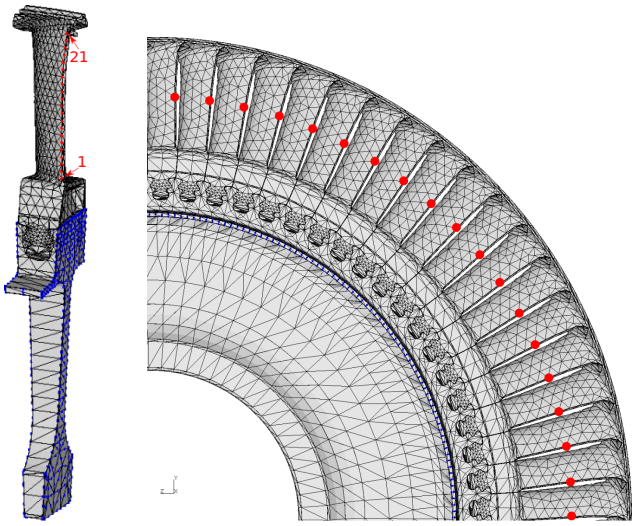

(a) Single blade

(b) Quarter of the bladed disk

FIGURE 2: Finite element models

Single Blade

The finite element model consists of quadratic tetrahedral elements with approximately 19,000 nodes. The material of the disk segment is considered to be isotropic, and the blade material is orthotropic. Fixed boundary conditions have been applied on the two sides of the disk segment (blue nodes in Fig. 2a) and the contact interfaces of the shroud are not constrained. A centrifugal load of $8625 rpm$ has been applied and the static calculation has been carried out with nonlinear geometric effects included.

Effect of anisotropy axis scatter on the single blade natural frequencies In order to find a realistic range of the natural frequency variation due to crystal orientation scatter a set of simulations have been performed using the single blade finite element model. The total number of blades with different anisotropy orientation in this set is 10,000. The anisotropy angles of α, β and ζ have been randomly generated using statistical distributions based on measurements of single crystal orientation.

The first six natural frequency values of sample population have been normalized by the corresponding natural frequency values of the finite element model with the crystal orientation coinciding with the blade coordinate system.

In Fig. 3 the normalized frequency scatter of the sample population is shown, with the normalized value of 1 corresponding to a green triangle. The calculated mean value of the population is represented by filled blue circles in Fig. 3. One simulation has also been carried out by choosing the mean value of the statistical distributions described for the three anisotropy angle and setting the crystal orientation according to those values. These values are visualized in the figure by red circles.

In Fig. 3 it is shown that the first (1^{st} flap - 1F), the second

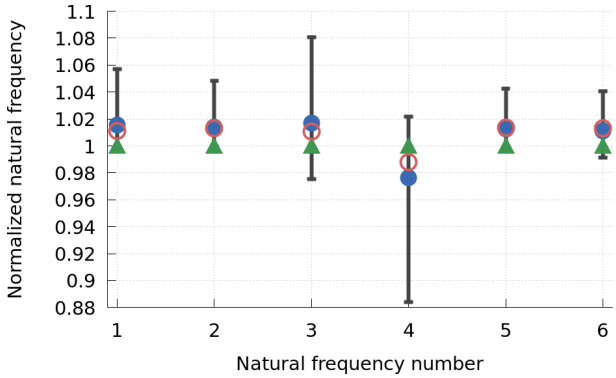

FIGURE 3: Normalized natural frequency of single blade with varied crystal orientation

(1^{st} edgewise - 1E), the fifth (2^{nd} edgewise - 2E) and sixth (3^{rd} edgewise - 3E) natural frequencies are increased by any deviation of the crystal orientation, the natural frequencies 3 (2^{nd} flap - 2F) and 4 (1^{st} torsional - 1T) can be increased or decreased. The largest range is 13.8% in case of mode 4 and the smallest range is 4.7% in case of mode 5. The mean values of the natural frequencies are close to the natural frequency of the blade when the anisotropy axis coincides with the stacking axis. From the figure it can be see that in the case of natural frequencies 2, 5 and 6, the value of the mean of the population and the blade with the crystal orientation based on the mean anisotropy angles is very close in value, however this is not valid for the other modes.

The examples of the dependency of natural frequencies on the crystal orientation are shown in Fig. 4 for the 1^{st}, 2^{nd} and 6^{th} modes. The primary angle α and the secondary angle β were changed, while the angle ζ was kept constant at $0°$. The natural frequency values are normalized with the natural frequency calculated with the crystal orientation based on the angles $\alpha = \beta = \zeta = 0°$.

For the first two modes the lowest values are occurring when the crystal coordinate system coincides with the stacking axis. For these modes the increasing primary angle α causes a monotonous increase in the natural frequencies. The values of the natural frequencies of mode 6 show a more complex behavior.

Validation of the sensitivity of modal characteristics with respect to the anisotropy angles The sensitivities of the natural frequencies calculated with the semi-analytic method are compared with the values obtained by the finite difference method. The calculation of the approximation of the derivatives by the finite difference method is performed as:

$$\frac{\partial f}{\partial \Gamma_i} \approx \frac{f(\Gamma_i + \Delta\Gamma_i) - f(\Gamma_i)}{\Delta\Gamma_i} \tag{38}$$

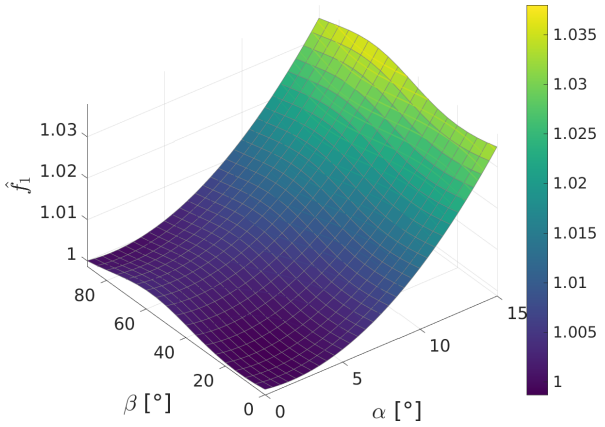

(a) Normalized natural frequency 1 (1F)

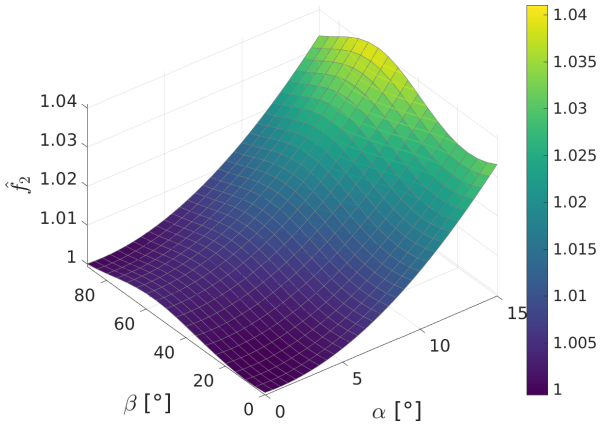

(b) Normalized natural frequency 2 (1E)

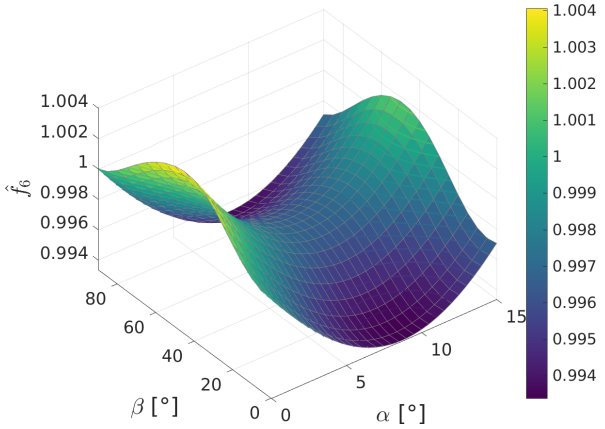

(c) Normalized natural frequency 6 (2E)

FIGURE 4: Normalized natural frequency of three modes with varying crystal orientation

where $\Delta\Gamma_i = 0.001 rad$. It should be noted that the finite difference approximation allows the verification the implementation of the new method, however its accuracy is generally lower in comparison with the new method. The reason for this is the limited

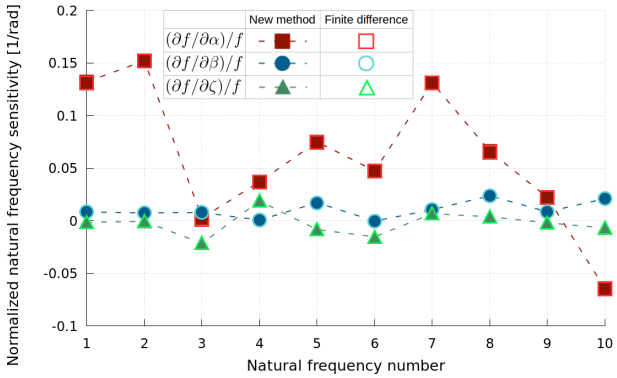

FIGURE 5: Normalized natural frequency sensitivities with respect to anisotropy angles

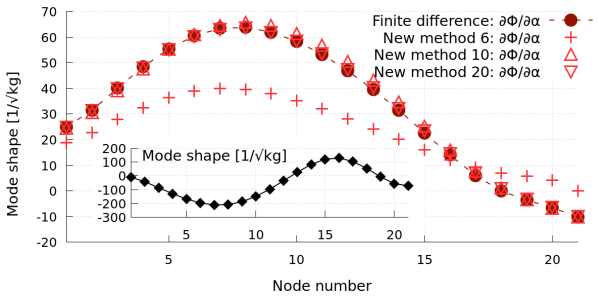

FIGURE 6: Validation results of the sensitivity of mode shape 6 (3E) with respect to α

precision of the natural frequency and mode shape values, used in Eq. (38).

The sensitivities of the first ten natural frequencies of the single blade were calculated. The sensitivities were obtained with respect to all three anisotropy angles. An example of the validation is shown in Fig. 5. The normalized natural frequency results calculated with the new method reveal a good correspondence when compared with the values obtained by the finite difference method. The sensitivities with respect to the primary angle α are the most significant for almost all modes. The sensitivity values with respect to β and ζ are smaller. The largest value of the normalized sensitivity of natural frequency is $(\partial f_2/\partial\alpha) = 15.2\,\%/rad = 0.084\,\%/deg$.

The convergence characteristics of the mode shape sensitivities are demonstrated by comparing the sensitivities at the nodes of the trailing edge of the blade, where the first node is the one closest to the root of the blade and the last node near the tip, see Fig. 2a. The sensitivity of mode shape 6 is calculated with respect to the anisotropy angle α and with different number of mode shapes kept in the expansion basis: 6, 10 and 20 modes. The mode shape and its sensitivity are shown in Fig. 6.

From Fig. 6 and from extensive studies, which are not provided here due to the restricted space, it can be seen that to ob-

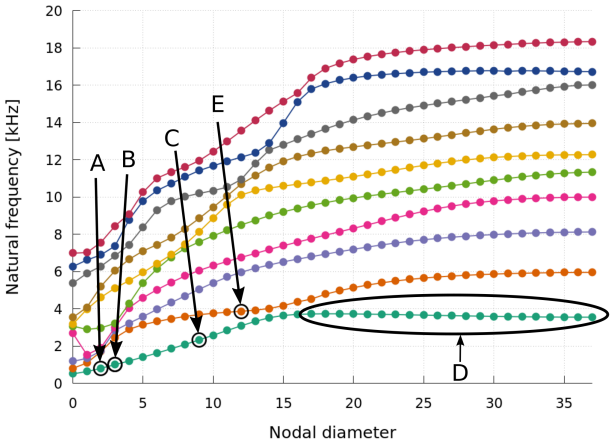

FIGURE 7: Natural frequency-nodal diameter diagram of the cyclic symmetric bladed disk model with full contact on the shrouds

tain the sensitivity of mode shapes with sufficient precision, the number of mode in the expansion basis should be approximately double the mode number at least for the case of a single blade analysis.

Mistuned Bladed Disk

For the analysis of a mistuned bladed disk a full model of a bladed disk with 75 blades has been created. The random mistuning pattern was generated using realistic statistical distribution provided by the blade manufacturer for all the anisotropy angles. The details of these distributions are not provided here due to confidentiality restrictions. The finite element model consists of approximately 0.5 million nodes. The nodes shown in blue in Fig. 2b have fixed boundary conditions applied in axial and tangential directions. At the contact interfaces on the fir-tree full contact and on the shrouds different contact conditions are applied: (i) full contact, (ii) sliding contact and (iii) no contact. The static analysis is performed with nonlinear geometric effects included and the static stress distribution are used as a perturbation for the subsequent modal analysis step. For the analysis, low and high nodal diameter, and localized modes are selected, see (A)-(D) in Fig. 7. The sensitivities of the mode shapes are calculated with 200 modes included in the basis of expansion, therefore the sensitivity of the mode shapes (A)-(D) can be captured with sufficient precision.

Effect of anisotropy axis scatter on the bladed disk mode shapes In the previous section it has been discussed how the crystal orientation can influence the natural frequencies of the stand-alone blade. In this section the effect of the varying crystal orientations is demonstrated with a set of modal analyses calculations with 50 different anisotropy mistuning patterns. In Fig. 8 the axial displacement of the mode shape is shown at the node on the mid-span of the trailing edge on each blade, see Fig. 2b. From the 50 different simulation, ten is shown in Fig. 8. Additionally, the tuned mode shapes with anisotropy angles $\alpha = \beta = \zeta = 0^\circ$ are plotted on these graphs with black circles.

It has been found that the higher nodal diameter mode shapes and the localized mode shapes are more sensitive to crystal orientation variations. The effect of different anisotropy angle mistuning is shown in Fig. 8.

In case of mode A, see Fig. 8a, selected from the first family of modes with two nodal diameters, the mode shape is shifted around the circumference of the bladed disk.

The results show similar behavior for mode (C) in Fig. 8b, that is a mode from the first family with nine nodal diameters. The mode shapes are shifted around the circumference of the bladed disk and the nodal diameter pattern is distorted.

Fig.8c shows how the mode number 76 (one of the modes from range (D) in Fig.7) changes with changing the anisotropy mistuning pattern. The nodal diameter pattern is very distorted and results in a localized mode shape. Due to the high distortion of the mode shape caused by the anisotropy mistuning, no tuned mode shape is plotted in Fig. 8c. For each mistuning pattern the localization of the mode shape occurs at different blades and the largest values of the mode shape displacements vary.

Validation of the Sensitivity of Natural Frequencies for a Bladed Disk The sensitivities of the natural frequencies have been validated by the comparison with the finite difference method. The natural frequency sensitivities have been normalized by the natural frequencies.

The results of the validation for the first 200 modes in Fig. 9a and for selected higher natural frequency sensitivities in Fig. 9b, show a good correspondence with the finite difference reference approximation values. The sensitivities are shown here with respect to anisotropy angles α, β and ζ of blade 5. This figure, as well as other calculations that have been performed, show that the influence of the primary and the secondary angles are the most significant. In comparison, the sensitivity to the ζ angle is negligible.

Validation of the Sensitivity of Mode Shapes for a Bladed Disk The validation of the sensitivity of mode shapes are represented here with two examples.

The sensitivity of a localized mode shape from the first family, group (D) in Fig. 7, is shown with respect to the three anisotropy angles of the blade with the highest modal displacement of the blades in the bladed disk assembly. The nodal values are determined at the mid-span of the trailing edge of each blade, see nodes shown by red circles in Fig. 2b. The sensitivity results are compared with the finite difference values. The mode shape, considered in this example, is mode number 70.

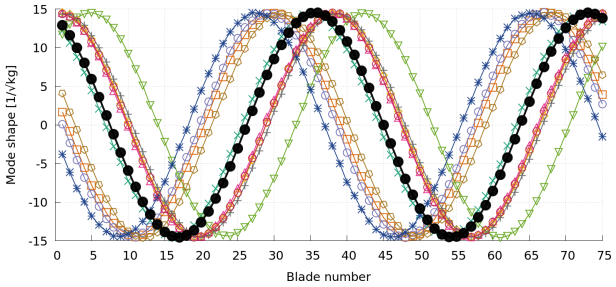

(a) Mode shape A

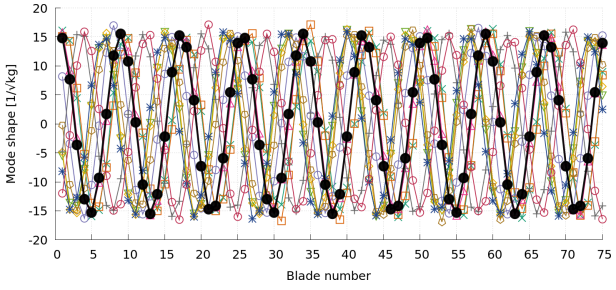

(b) Mode shape C

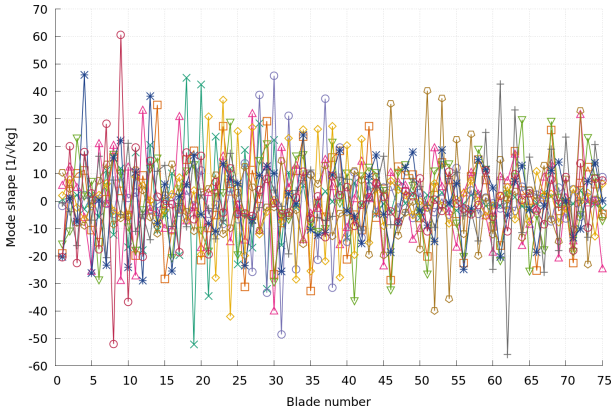

(c) Mode shape D

FIGURE 8: Mode shape variation for different anisotropy mistuning patterns

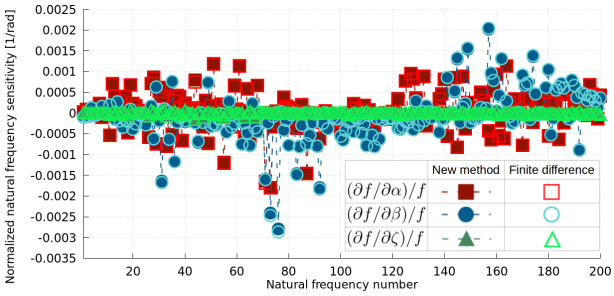

(a) First 200 modes

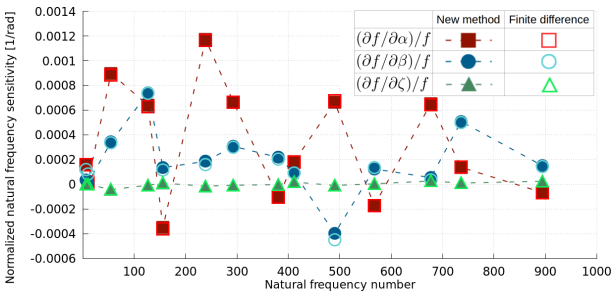

(b) Selected modes from the first 12 families

FIGURE 9: Validation of sensitivity of natural frequencies with respect to the anisotropy angles of blade 5

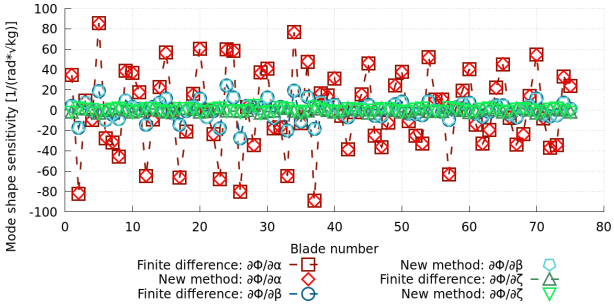

FIGURE 10: Validation of the sensitivity of mode shape D (70) with respect to the anisotropy angles of blade 5

The results of Fig. 10 show that the new method provides the same numerical values for the sensitivities of the mode shape as the finite difference method.

The sensitivities of the mode shapes have been validated for higher mode shapes arbitrarily selected from the first 12 family of modes. The sensitivities are calculated with respect to various rotation vector components of blade number 42 defined in the global CS. In Fig. 11 normalized mode shape sensitivity errors are shown as a function of number of mode shapes used in the basis. The relative error has been calculated as:

$$\varepsilon = \frac{(\partial \boldsymbol{\phi}/\partial r_i)_{New\ method} - (\partial \boldsymbol{\phi}/\partial r_i)_{Finite\ difference}}{(\partial \boldsymbol{\phi}/\partial r_i)_{Finite\ difference}} \qquad (39)$$

The sensitivities have been calculated with an increasing number of mode shapes included in the basis of the series expansion. From Fig. 11 it can be concluded that a very fast convergence can be achieved with the enhanced method implemented. The error reduces below 3% in the examples selected here, which is satisfactory considering that the reference value calculated with the finite difference is less accurate than the results obtained with the new method.

The sensitivities with respect to an anisotropy angle of any of the blade orientations can be illustrated also on all the nodes of the bladed disk. Fig. 12 shows mode shape 70 (D) and its sensitivity with respect to primary angle α of blade 25, where the mode localization occurs. The sensitivity of this localized mode shape, see Fig. 12b, has high values along the circumference of

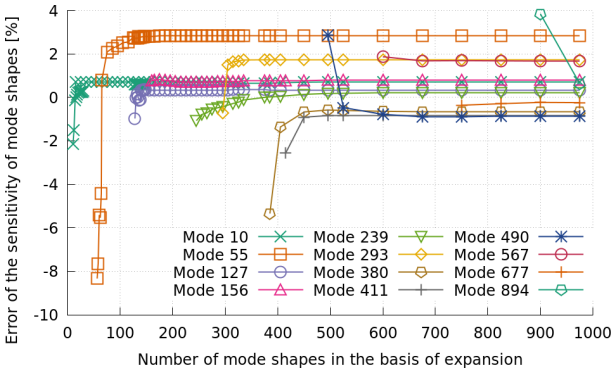

FIGURE 11: Error of the sensitivity of mode shapes for higher modes with respect to rotation vector components of blade 42

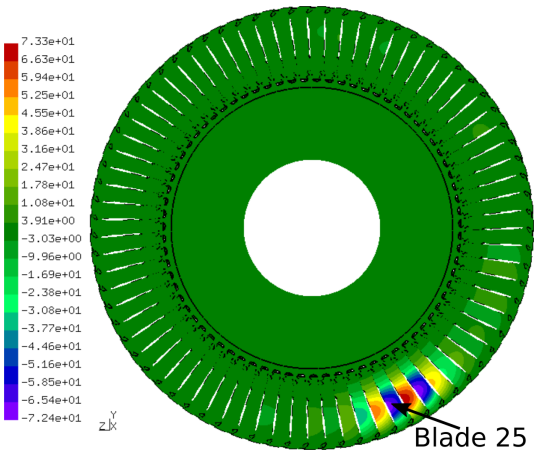

(a) Mode shape

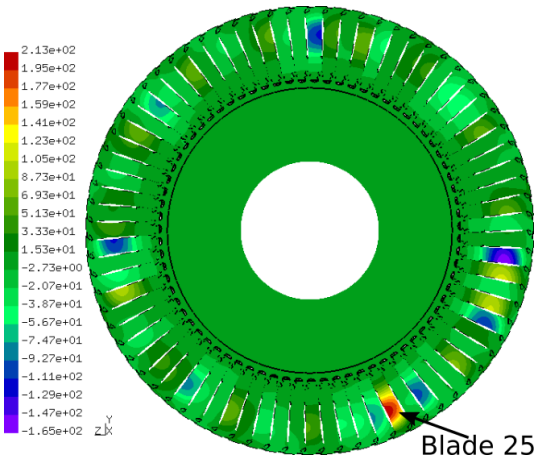

(b) Mode shape sensitivity

FIGURE 12: Mode shape D (70) and its sensitivity with respect to anisotropy angle α of blade 25

the bladed disk and not only at the blades where the localization occurs.

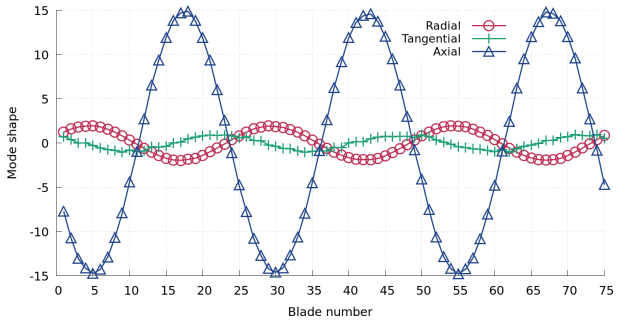

(a) Mode shape B

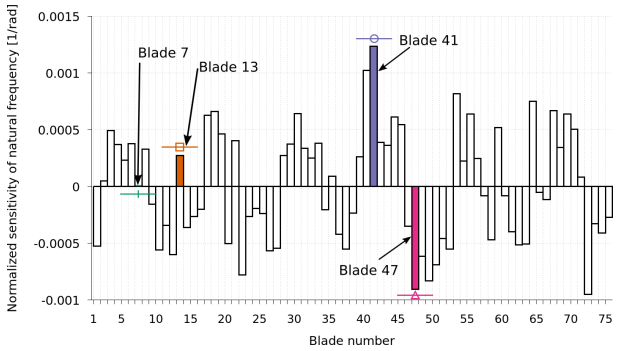

(b) Sensitivity of natural frequency to α angles

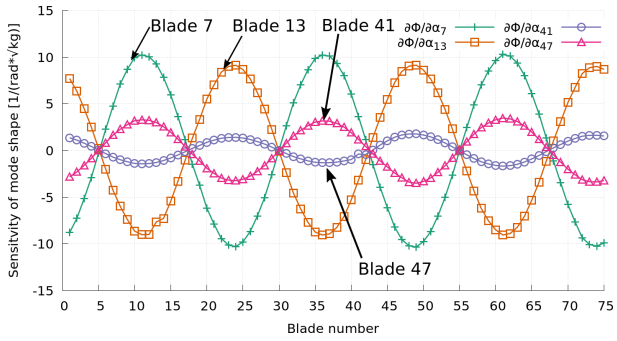

(c) Sensitivity of axial mode shape to selected α angles

FIGURE 13: Mode shape B: sensitivity of modal characteristics

Investigation of the Sensitivity of the Modal Characteristics The phenomena of the sensitivities of the modal characteristics with respect to the anisotropy angles is presented with three typical examples. In order to gain a comprehensive overview of the behavior of the sensitivities of the modal characteristics, the sensitivity of the natural frequencies and the mode shapes are analyzed together with the mode shapes. The sensitivities are shown with respect to the primary angle α.

In Fig. 13, a mode shape with 3 nodal diameters, (B) in Fig. 7, is investigated. The mistuning pattern does not visibly distort the sinusoidal nodal diameter mode shape. In Fig. 13b the normalized sensitivities of the natural frequency are plotted with respect to the α angle of the blade number shown on the

horizontal axis. The sensitivities of the mode shapes are shown with respect to selected primary angles. Two angles are chosen that have a high influence on the natural frequency (α angle of blade number 41 and 47) and two angles that have high effect on the mode shapes (α angle of blade number 7 and 13). The sensitivity of the mode shape with respect to the primary angles has extreme value where the mode shapes are zero and the sensitivities are zero where the mode shape has its maximum or minimum value.

The sensitivity of the modal properties of the localized mode shape of number 70, (D) in Fig. 7, from the first family of modes, see Fig. 14, is investigated. It can be seen that the highest sensitivities of the natural frequency are with respect to the primary angles of the blades where the mode localization occurs. The sensitivities with respect to α angles of blade 25, 26 and 28 has the highest sensitivity of natural frequencies and mode shapes values. Moreover, if a sensitivity of natural frequency has a small value, the mode shapes sensitivity values are also small with respect to the same α angle, see for example the primary angle of blade 50. It is worth mentioning that the mode shape sensitivities to the anisotropy angles have the highest values at the localization, however the whole mode shape is influenced by the change in crystal orientation. The numerical values of the sensitivities are at least one magnitude higher than the sensitivities in the case of mode (B).

A mode shape with high nodal diameter mode shape from the second family of modes (E) is shown in Fig. 15a. A distorted nodal diameter pattern can be identified, which means that this can be considered as a transition mode between the tuned mode shape and the localized modes. The sensitivities with respect to the primary angles of blade 72 and 75 are high for both natural frequencies and mode shapes, and blade 72 has both the maximum natural frequency and mode shape sensitivity values. In the transition modes, the angles with small natural frequency sensitivities can have significant influence on the mode shapes. For example, the primary angle of blade number 35 has a small influence on the natural frequency, however the sensitivity of the mode shape with respect to this angle cannot be neglected. The values of the sensitivities of the modal characteristics are in this case lower than what can be seen for the localized mode shape (D), but higher than the mode shape with a low number of nodal diameter (B).

In order to investigate which natural frequencies are the most sensitive to the orientation change of a single blade, the highest sensitivity of the natural frequency with respect to a single angle has been identified for each blade. The maximum and minimum numerical values of each normalized sensitivity of natural frequency with respect to all three anisotropy angles have been plotted in Fig. 16. The mode shapes of the first ten modes of the bladed disk are very close to the tuned mode shapes,and low sensitivity values can be observed. The modes from 25 to 69 are transition modes, where distorted nodal diameter patterns can

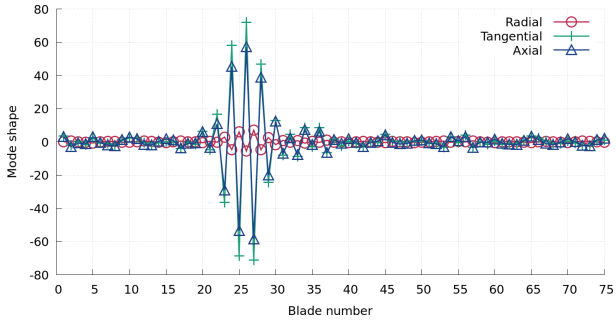

(a) Mode shape 70 (D)

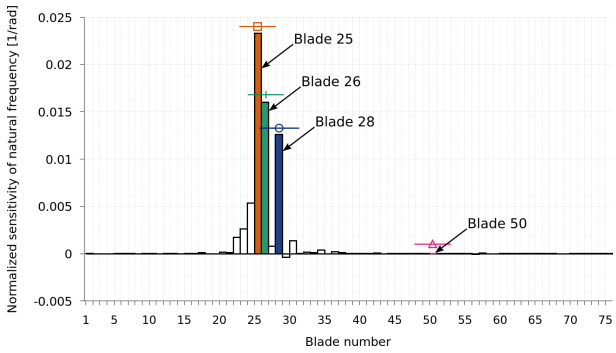

(b) Sensitivity of natural frequency to α angles

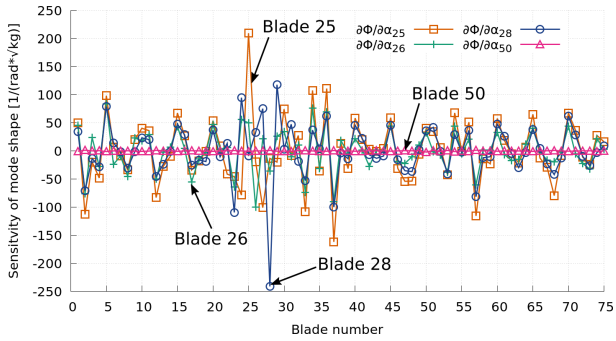

(c) Sensitivity of tangential mode shape to selected α angles

FIGURE 14: Mode shape 70 (D): sensitivity of modal characteristics

be identified. The modes from 70 to 80 have strongly localized mode shapes, with a high sensitivity of the natural frequencies to a small number of anisotropy angles. Results of the calculation show the highest positive values with respect to the anisotropy angle α. The secondary angle β can both increase and decrease the natural frequencies. The third anisotropy angle ζ has the smallest influence on most modes.

The bladed disk natural frequency sensitivities are investigated with different contact conditions: (ii) sliding contact and (iii) no contact between shrouds. In Fig. 17 the maximum and minimum values of sensitivities of the first 80 natural frequencies are shown with sliding condition on the shrouds. It is shown

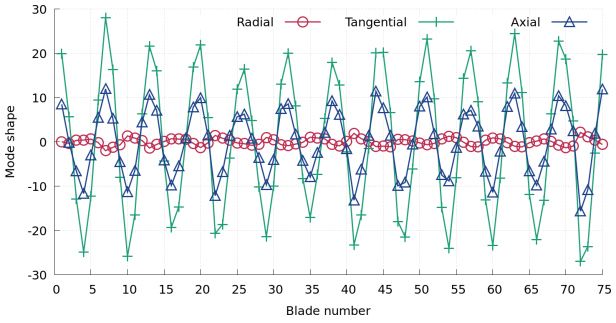

(a) Mode shape E

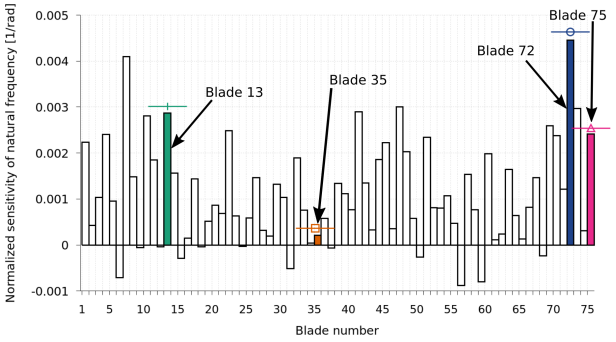

(b) Sensitivity of natural frequency to α angles

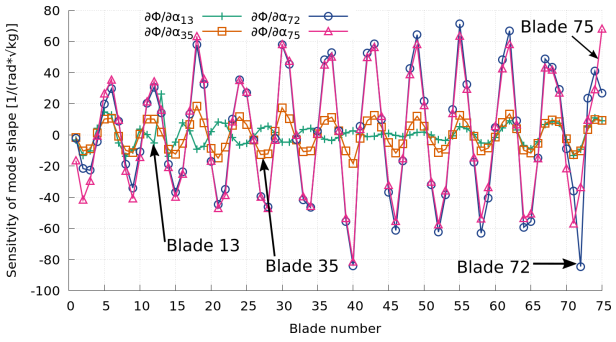

(c) Sensitivity of tangential mode shape to selected α angles

FIGURE 15: Mode shape E: sensitivity of modal characteristics

that the mode shape localization occurs for lower modes, which increases the sensitivity of the natural frequencies with respect to the primary angles with one order of magnitude. It can be observed that the effect of the circular angle ζ increases as the sensitivities with respect to α increase. In Fig. 17 it is visible that the sensitivity values with respect to ζ can be higher than the sensitivities to β.

In Fig. 18 the maximum and minimum values of the sensitivities of the natural frequencies are investigated without contact on the shrouds. The maximum sensitivity with respect to the primary angle α increases compared those observed with sliding contact conditions. The influence of the secondary angle β is not negligible compared to the sensitivities with respect to ζ.

A set of simulations has been carried out with the bladed

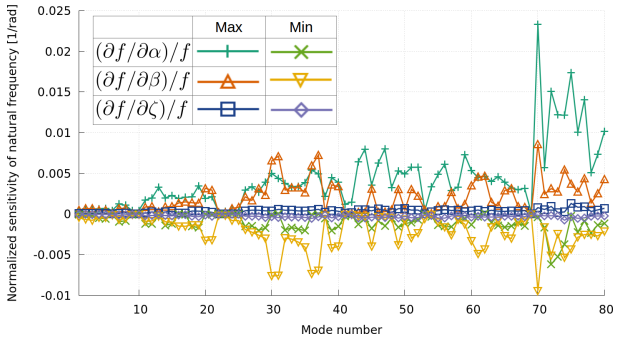

FIGURE 16: Highest value of the normalized natural frequencies with stick contact on the shroud

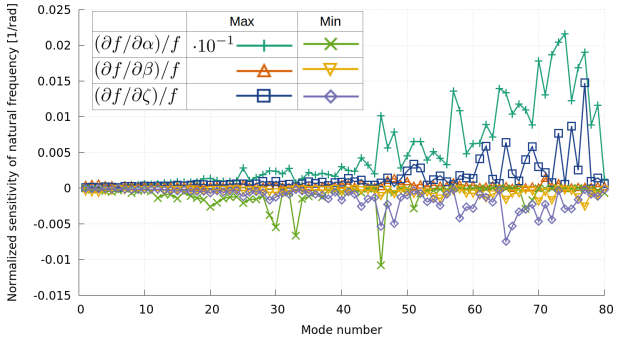

FIGURE 17: Highest value of the normalized natural frequencies with sliding contact on the shroud

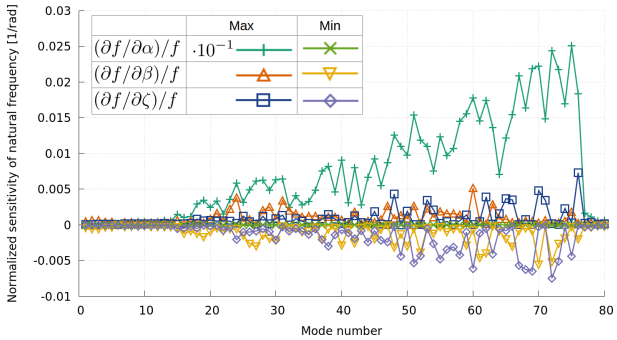

FIGURE 18: Highest value of the normalized natural frequencies with no contact on the shroud

disk model with stuck contact conditions on the shroud interfaces using ten different anisotropy mistuning patterns. In Fig. 19 the maximum and minimum values are shown for each mode with respect to the primary angle α. The highest values of the natural frequency sensitivities calculated with the different mistuning patterns are very close in numerical values for the lower modes. For the modes higher than 70, that are strongly localized, the maximum and minimum values of the natural frequency sensitivity strongly vary for different mistuning patterns.

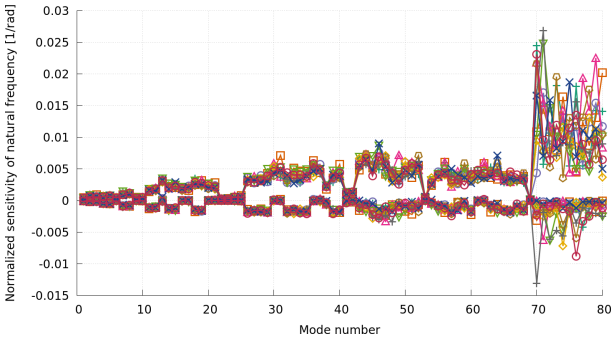

FIGURE 19: Highest value of the normalized natural frequency sensitivities to α for ten different mistuning pattern and with stuck contact on the shroud

CONCLUSIONS

A method has been developed for the evaluation of the local sensitivities of the modal properties with respect to the parameters describing the material anisotropy in the blades of a bladed disk assembly. The method enables a fast and reliable calculation of the sensitivities of bladed disks.

The enhanced method developed for the calculation of the sensitivities of the mode shapes shows good convergence characteristics for lower and higher modes.

A method for transforming the sensitivities to the manufacturer coordinate system using an analytic derivation has been developed.

The method has been validated with the examples of a single blade and a bladed disk. The analysis of the sensitivity of the mode shapes showed that the localized mode shapes of the mistuned bladed disk are the most sensitive to the change in the crystal orientation. In case of the localized mode shapes the sensitivities with respect to the anisotropy angles of the blades where localization occurs can highly influence both natural frequencies and mode shapes.

The qualitative characteristics of the effect of the anisotropy orientation have been obtained for realistic single blade and mistuned bladed disk assemblies. The study of the effect of the different boundary conditions of the shrouded blade disk on the natural frequency sensitivities has been performed.

ACKNOWLEDGMENT

The authors are grateful for MTU Aero Engines AG for their financial support provided for this project and for the permission to publish this work.

REFERENCES

[1] Arakere, N. K., and Swanson, G., 2002. "Effect of crystal orientation on fatigue failure of single crystal nickel base turbine blade superalloys". *Journal of Engineering for Gas Turbines and Power-Transactions of the Asme,* ***124***(1), Jan., pp. 161–176.

[2] Dong, C., Yu, H., Li, Y., Yang, X., and Shi, D., 2014. "Life modeling of anisotropic fatigue behavior for a single crystal nickel-base superalloy". *International Journal of Fatigue,* ***61***, pp. 21–27.

[3] Savage, M. W. R., 2011. "The Influence of Crystal Orientation on the Elastic Stresses of a Single Crystal Nickel-Based Turbine Blade". *Journal of Engineering for Gas Turbines and Power,* ***134***(1), Oct., pp. 012501–012501–7.

[4] Manetti, M., Giovannetti, I., Pieroni, N., Horculescu, H., Peano, G., Zonfrillo, G., and Giannozzi, M., 2009. "The dynamic influence of crystal orientation on a second generation single crystal material for turbine buckets". In Proceedings of the ASME Turbo Expo, Vol. 6, pp. 125–133.

[5] Kaneko, Y., 2011. "Study on vibration characteristics of single crystal blade and directionally solidified blade". In Proceedings of the ASME Turbo Expo, Vol. 6, pp. 931–940.

[6] Kaneko, Y., Mori, K., and Ooyama, H., 2015. "Resonant response and random response analysis of mistuned bladed disk consisting of directionally solidified blade". In Proceedings of the ASME Turbo Expo, Vol. 7B.

[7] Feiner, D. M., and Griffin, J. H., 2002. "A Fundamental Model of Mistuning for a Single Family of Modes". *Journal of Turbomachinery,* ***124***(4), Nov., pp. 597–605.

[8] Adelman, H., and Haftka, R., 1986. "Sensitivity analysis of discrete structural systems". *AIAA Journal,* ***24***(5), pp. 823–832.

[9] Amors, J. L., Buerger, M. J., and de Amors, M. C., 1975. *The Laue Method.* Academic Press, New York.

[10] Dhondt, G., 2017. *CalculiX CrunchiX USERS MANUAL version 2.12*.

[11] Cardona, A., and Geradin, M., 1988. "A beam finite element non-linear theory with finite rotations". *International Journal for Numerical Methods in Engineering,* ***26***(11), pp. 2403–2438.

[12] Petrov, E., and Geradin, M., 1998. "Finite element theory for curved and twisted beams based on exact solutions for three-dimensional solids. Part 1: Beam concept and geometrically exact nonlinear formulation". *Computer Methods in Applied Mechanics and Engineering,* ***165***(1-4), pp. 43–92.